Schweizerischer Erdbebendienst
Service Sismologique Suisse
Servizio Sismico Svizzero
Servizi da Terratrembels Svizzer

ETH
Eidgenössische Technische Hochschule Zürich
Swiss Federal Institute of Technology Zurich

Solothurn - Brühl (SOLB)

SITE CHARACTERIZATION REPORT

Clotaire MICHEL, Jan BURJANEK, Valerio POGGI,

Daniel ROTEN, Carlo CAUZZI, Donat FÄH

Sonneggstrasse 5 CH-8092 Zürich Switzerland; E-mail: clotaire.michel@sed.ethz.ch

Last modified : November 5, 2013

Abstract

Ambient vibration array measurements were performed on the alluvial site of Solothurn Brühl. The site, where the new station SOLB of the Swiss Strong Motion Network was installed, is located on loose glacial-lacustrine quaternary sediments of the former lake Solothurn. In order to characterize the velocity profile under the station, array measurements with a $240\,\mathrm{m}$ aperture were performed. The measurements were successful and allowed deriving a velocity model for this site. The soil column underlying station SOLB is made of weak lacustrine sediments of about $10\,\mathrm{m}$ with a shear wave velocity of about $200\,\mathrm{m/s}$. Below, moraine sediments with V_s from 370 to $600\,\mathrm{m/s}$ can be found down to an interface at $180\,\mathrm{m}$. This interface corresponds to the interface with the Molasse rock. The velocity in the Molasse is not constrained. Moreover, 2D resonance of the basin is suspected but the amplitude of the polarization is too low to definitely conclude. $V_{s,30}$ is found to be close to $274\,\mathrm{m/s}$. The EC8 and SIA261 ground types are C and D, respectively. Recordings on the new station will allow to validate the proposed 1D models and quantify the eventual 2D effects.

Contents

1 Introduction

The station SOLB (Solothurn Brühl) is part of the Swiss Strong Motion Network (SSMNet) on the Swiss Plateau region. SOLB has been installed in the framework of the SSMNet Renewal project in 2012 as a new site. This project covers also the site characterization. The passive array measurement has been selected as a standard tool to investigate these sites. Such a measurement campaign was carried out on 16th May 2012 close to the Brühl school (Fig. 1), with a centre $120\,\mathrm{m}$ South of station SOLB, in order to characterize the sediments under this station. The station is located on soft glacial-lacustrine sediments (so-called former "lake Solothurn") in the deep Aar basin, according to the geological map. This report presents the measurement setup, the results of the H/V analysis and of the array processing of the surface waves, aimed at estimating the dispersion curves. Then, an inversion of these results for a velocity profile is performed. Standard parameters are derived to evaluate the amplification at this site.

Canton	City	Location	Station code	Site type	Slope
Solothurn	Solothurn	Brühl	SOLB	Alluvial plain	Flat

Table 1: Main characteristics of the study-site.

Figure 1: Picture of the site.

2 Experiment description

2.1 Ambient Vibrations

The ground surface is permanently subjected to ambient vibrations due to:

- natural sources (ocean and large-scale atmospheric phenomena) below $1\,\mathrm{Hz}$,
- local meteorological conditions (wind and rain) at frequencies around $1\,\mathrm{Hz}$,
- human activities (industrial machines, traffic…) at frequencies above $1\,\mathrm{Hz}$ [Bonnefoy-Claudet et al., 2006].

The objective of the measurements is to record these ambient vibrations and to use their propagation properties to infer the underground structure. First, the polarization of the recorded waves (H/V ratio) is used to derive the resonance frequencies of the soil column. Second, the arrival time delays at different stations are used to derive the velocity of surface waves at different frequencies (dispersion). The information (H/V, dispersion curves) is then used to derive the properties of the soil column using an inversion process.

2.2 Equipment

For these measurements, 12 Quanterra Q330 dataloggers named NR01 to NR12 and 14 Lennartz 3C 5 s seismometers were used (see Tab. 2). Each datalogger can record on 2 ports A (channels EH1, EH2, EH3 for Z, N, E directions) and B (channels EH4, EH5, EH6 for Z, N, E directions). Time synchronization was ensured by GPS. The sensors were placed on a metal tripod, generally on the asphalt for this measurement.

Digitizer	**Model**	**Number**	**Resolution**
	Quanterra Q330	12	$24\,\mathrm{bits}$
Sensor type	**Model**	**Number**	**Cut-off frequency**
Velocimeter	Lennartz 3C	14	$0.2\,\mathrm{Hz}$

Table 2: Equipment used.

2.3 Geometry of the arrays

Two array configurations were used, for a total of 4 rings of 15, 30, 60 and $120\,\mathrm{m}$ radius around a central station. The first configuration includes the 3 inner rings with 14 sensors; the second configuration includes the 2 outer rings with 11 sensors with an additional sensor of the first ring that was not removed. The minimum inter-station distance and the aperture are therefore 15 and $120\,\mathrm{m}$ and 15 and $240\,\mathrm{m}$, respectively. The experimental setup is displayed in Fig. 2. The final usable datasets are detailed in section 3.2.

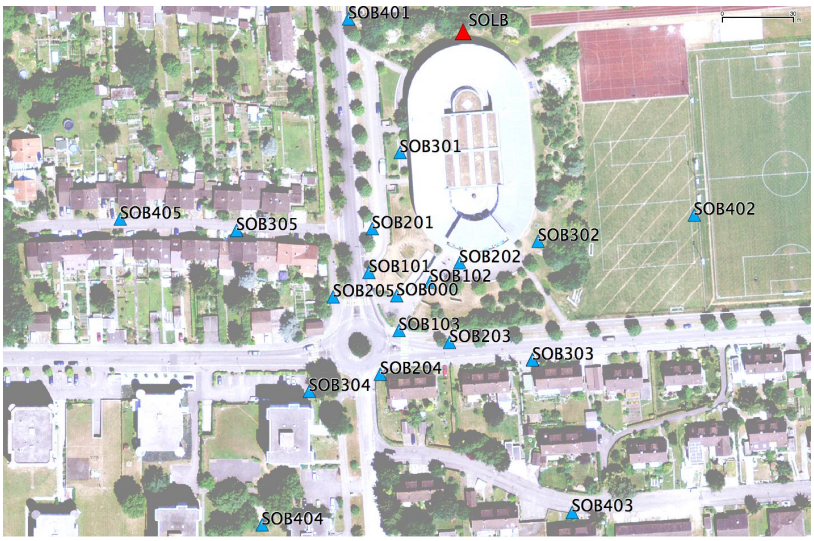

Figure 2: Geometry of the arrays.

2.4 Positioning of the stations

The sensor coordinates of the array were measured using a differential GPS device (Leica Viva), including only a rover station and using the Real Time Kinematic technique provided by Swisstopo. It allows an absolute positioning with an accuracy of about $3\,\mathrm{cm}$ on the Swissgrid. For, some of the points below trees, this accuracy was not reached but it was always better than $7\,\mathrm{cm}$ except for point SOB203 ($12.5\,\mathrm{cm}$).

3 Data quality

3.1 Usable data

The largest time windows were extracted, for which all the sensors of the array were in position and the GPS synchronization was ensured. Wind $10 - 20\,\mathrm{km/h}$ was blowing during the whole measurement and showers also occurred. Station NR08 failed writing large portions of signals on the Baler so the recordings are very short at point SOB303 for dataset 1. It was removed from the SAC dataset. Traffic through the array is clearly noticeable above $10\,\mathrm{Hz}$ on the spectra. The wind affects the spectra below $0.8\,\mathrm{Hz}$. Component E of point SOB302 failed. The characteristics of the datasets are detailed in Tab. 3.

3.2 Data processing

The data were first converted to SAC format, including in the header the sensor coordinates (CH1903 system), the recording component and a name related to the position of the station. The name is made of 3 letters characterizing the location (SOB here), 1 digit for the ring and 2 more digits for the number in the ring. Recordings were not corrected for the instrumental response.

Dataset	Starting Date	Time	Length	F_s	Min. inter-distance	Aperture	# of points
1	2012/05/16	10:20	123 min	200 Hz	15 m	120 m	13
2	2012/05/16	12:55	123 min	200 Hz	15 m	240 m	12

Table 3: Usable datasets.

4 H/V processing

4.1 Processing method and parameters

In order to process the H/V spectral ratios, several codes and methods were used. The classical H/V method was applied using the Geopsy `http://www.geopsy.org` software. In this method, the ratio of the smoothed Fourier Transform of selected time windows are averaged. Tukey windows (cosine taper of 5% width) of $50\,\mathrm{s}$ long overlapping by 50% were selected. Konno and Ohmachi [1998] smoothing procedure with b=80 was used. The classical H/V of Fäh et al. [2001] was also applied.

Moreover, the time-frequency analysis method [Fäh et al., 2009] was used to estimate the ellipticity function more accurately using the Matlab code of V. Poggi, available in the software repository of the engineering seismology group of SED. In this method, the time-frequency analysis using the Wavelet transform is computed for each component. For each frequency, the maxima over time (10 per minute with at least $0.1\,\mathrm{s}$ between each) in the TFA are determined. The Horizontal to Vertical ratio of amplitudes for each maximum is then computed and statistical properties for each frequency are derived. A Cosine wavelet with parameter 9 was used. The mean of the distribution for each frequency is stored. For the sake of comparison, the time-frequency analysis of Fäh et al. [2001], based on the spectrogram, was also used, as well as the wavelet-based TFA coded in Geopsy.

The ellipticity was also extracted using the Capon analysis [Poggi and Fäh, 2010] (see section on 3C array analysis) and also plotted on Fig. 6.

Method	Freq. band	Win. length	Anti-trig.	Overlap	Smoothing
Standard H/V Geopsy	$0.2 - 20\,\mathrm{Hz}$	$50\,\mathrm{s}$	No	50%	K&O 80
Standard H/V D. Fäh	$0.2 - 20\,\mathrm{Hz}$	$30\,\mathrm{s}$	No	75%	?
H/V TFA Geopsy	$0.2 - 20\,\mathrm{Hz}$	Morlet m=8 fi=1	No	-	?
H/V TFA D. Fäh	$0.2 - 20\,\mathrm{Hz}$	Specgram	No	-	?
H/V TFA V. Poggi	$0.2 - 20\,\mathrm{Hz}$	Cosine wpar=9	No	-	No

Table 4: Methods and parameters used for the H/V processing.

4.2 Results

A peak around $0.6\,\mathrm{Hz}$ is found in most of the recordings of the array but it could be due to wind. Results of a long term station XSOL3 recording in the school building is therefore necessary to interpret these results (Fig. 3). Fig. 4 shows that this peak frequency is indeed the fundamental frequency of Rayleigh waves. Variations in the array are only due to bad quality recordings (ground coupling) like in points SOB101, SOB203 (both located on grass) and SOB401. Point SOB402 is noticeably differing from the others but it is not clear whether it is due to disturbances (football players), coupling (located on grass) or an actual variation in the underground structure.

Moreover, an upper mode can be clearly seen around $5\,\mathrm{Hz}$ with variation in the array. Fig. 5 shows these variations: values are the largest to the South (up to $7\,\mathrm{Hz}$), around $5\,\mathrm{Hz}$ in the

central part, with a local minima in between at $4.3\,\mathrm{Hz}$ and smallest to the East and to the West (around $3.6 - 3.9\,\mathrm{Hz}$), the recordings close to the school building do not show any peak. It may result from a shallower interface.

Moreover, all the methods to compute H/V ratios are compared on Fig. 6, in which the classical methods were divided by $\sqrt{2}$ to correct from the Love wave contribution [Fäh et al., 2001]. The matching is good except smoothing issues.

As a conclusion a the SOLB station site, the fundamental frequency in the H/V curve is found to be $0.6\,\mathrm{Hz}$ with an amplitude of 4 and a second peak is found around $4.5 - 5\,\mathrm{Hz}$.

The results of the 3C FK analysis are perfectly matching the results obtained with other techniques although the peak of the upper mode is smeared.

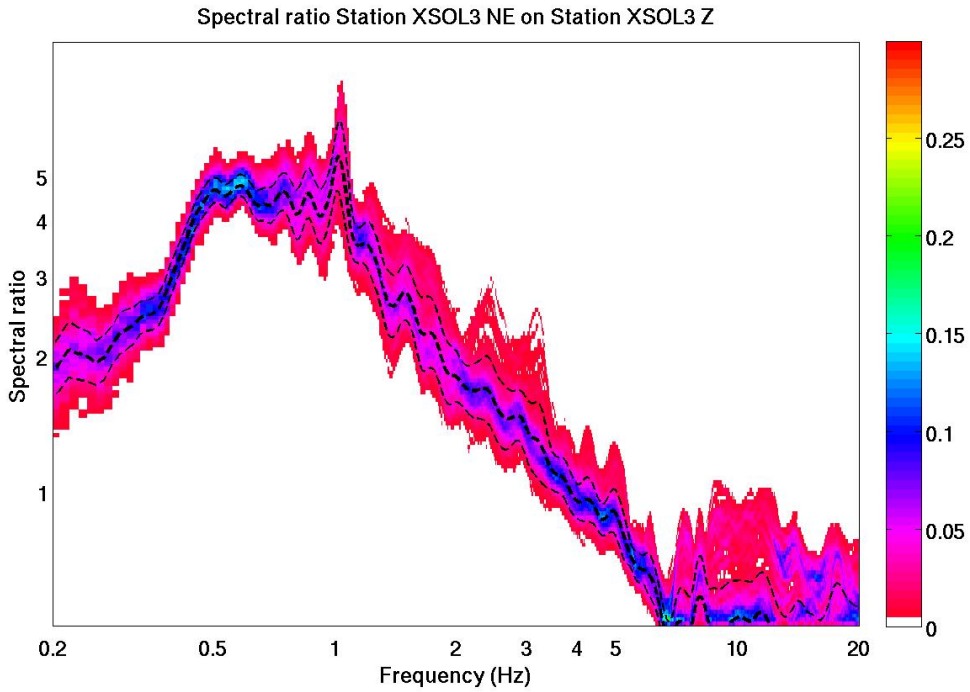

Figure 3: H/V spectral ratios on long time series at test station XSOL3. Color scale corresponds to occurrence of the H/V amplitude.

Considering the shape of the deep Aare basin, more variations of the fundamental frequency are expected, so a 2D resonance can be considered. Polarization analysis on the array data was performed using the method of Burjánek et al. [2010]. Most of the stations show a strong polarization on a broad frequency range perpendicularly to roads likely due to the air flow when cars are passing by. At some points (e.g. in the array centre Fig. 7), a weak polarization is noticed at $0.6\,\mathrm{Hz}$ in the direction of the Aare basin (E-W) but its amplitude is too low to definitely conclude. The results for 2 hours in the night at station XSOL3 are similar to the array centre. From Fig. 7, however, a clear polarization at the second peak ($5\,\mathrm{Hz}$) can be seen, but the strike is varying much across the array.

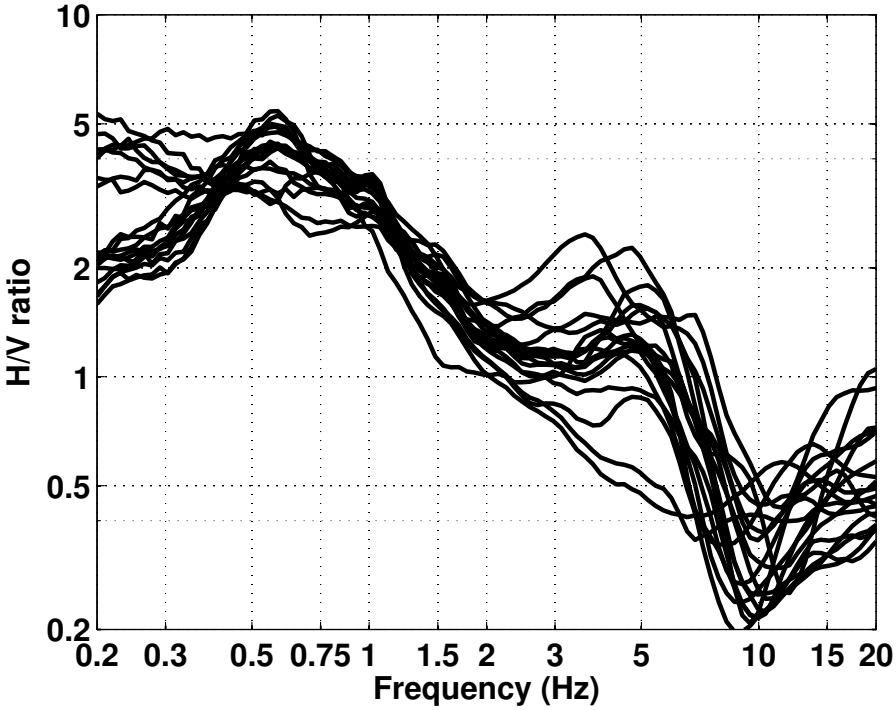

Figure 4: H/V spectral ratios (time-frequency analysis code V. Poggi).

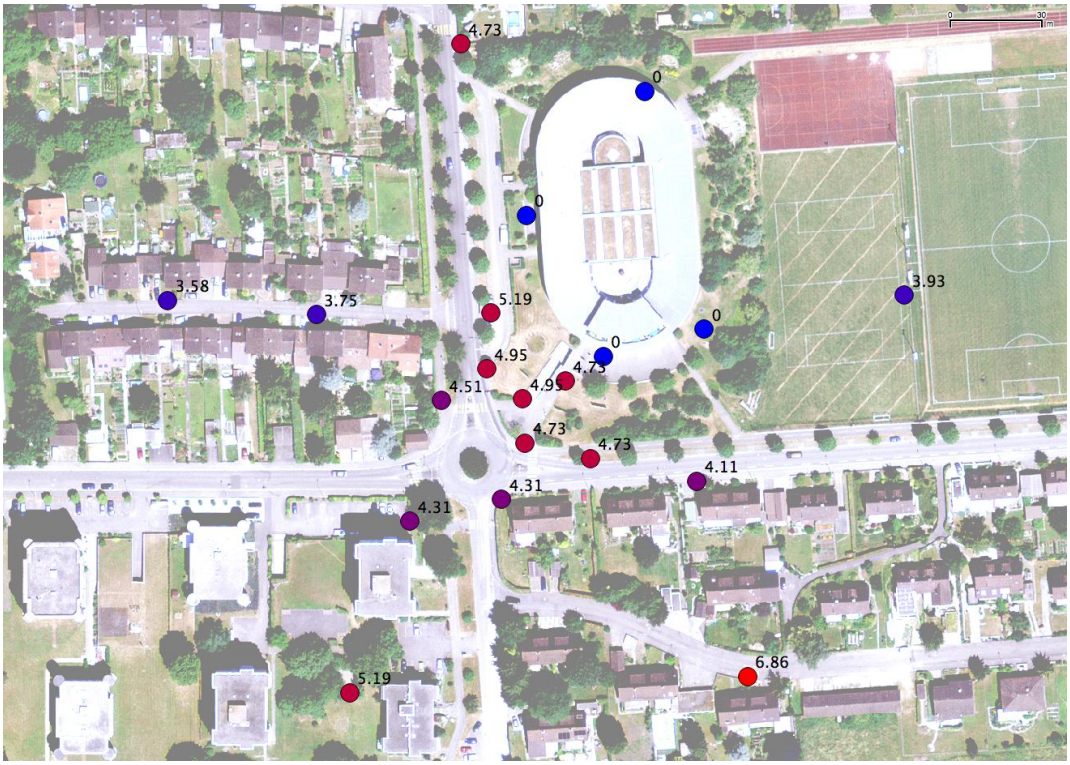

Figure 5: Map of the higher frequency peak (in Hz) of the H/V curves. 0 stands for no peak.

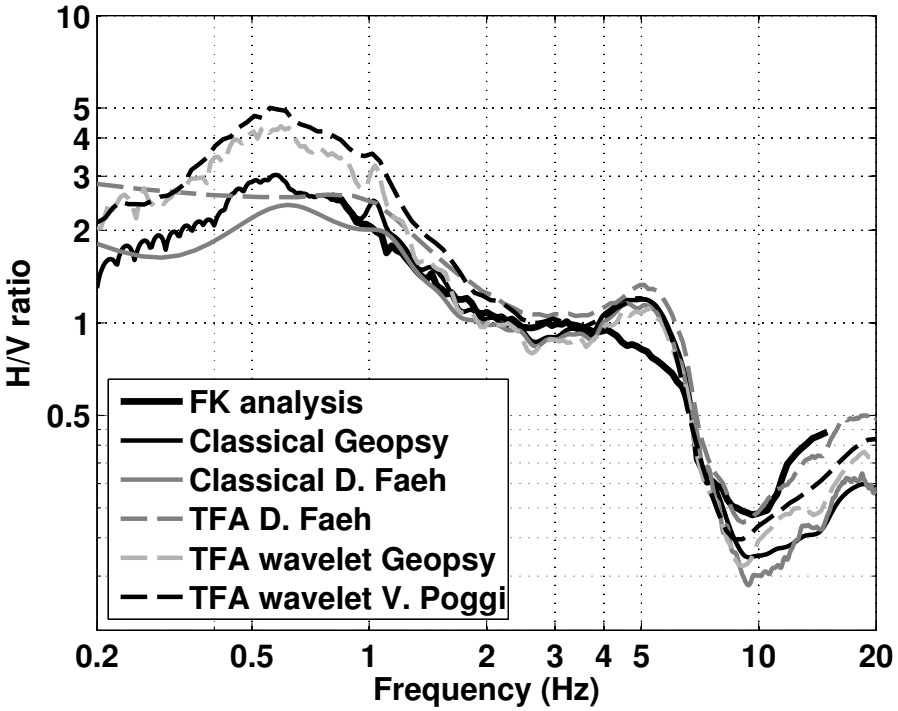

Figure 6: H/V spectral ratios for point SOB000 using the different codes. Classical methods were divided by $\sqrt{2}$.

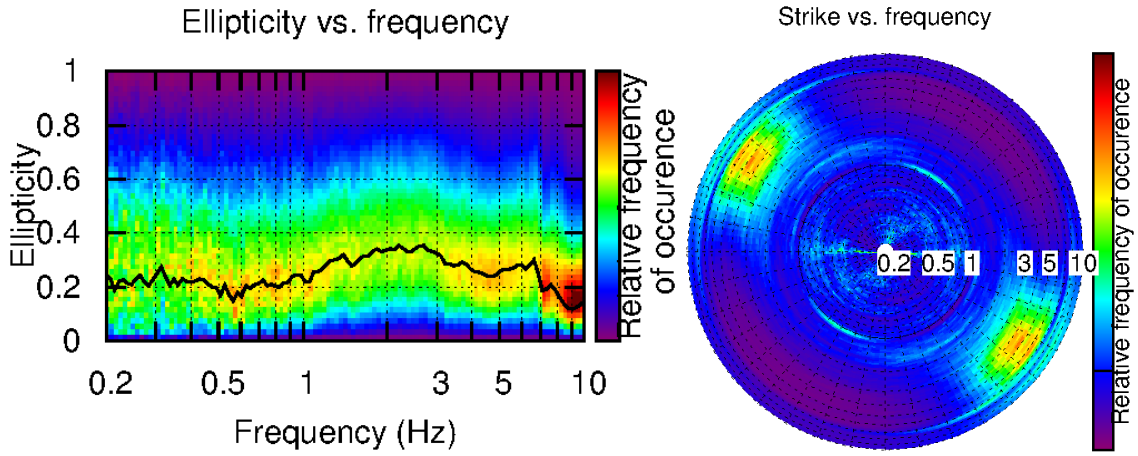

Figure 7: Polarization analysis at point SOB000. Left: Ellipticity (A trough in the ellipticity corresponds to polarized motion). Right: Strike of the polarization.

5 Array processing

5.1 Processing methods and parameters

The vertical components of the arrays were processed using the High-resolution FK analysis [Capon, 1969] using the Geopsy `http://www.geopsy.org` software. Better results were obtained using large time windows (300T). The results in the FK plane were concatenated.

Moreover, a 3C array analysis [Fäh et al., 2008] was also performed using the Array Tool 3C software [Poggi and Fäh, 2010] using the Capon SVD method. It allows to derive Rayleigh and Love modes. The results of computations of both datasets were merged to estimate the dispersion curves.

Method	Set	Freq. band	Win. length	Anti-trig.	Overlap	Grid step	Grid size	# max.
HRFK 1C	1	$0.8 - 15\,\mathrm{Hz}$	$300T$	No	50%	0.001	0.5	5
HRFK 1C	2	$0.8 - 15\,\mathrm{Hz}$	$300T$	No	50%	0.001	0.4	5
HRFK 3C	1	$0.8 - 15\,\mathrm{Hz}$	Wav. 10 Tap. 0.1	No	5%	50 m/s	2000 m/s	5
HRFK 3C	2	$0.8 - 15\,\mathrm{Hz}$	Wav. 10 Tap. 0.1	No	5%	50 m/s	2000 m/s	5

Table 5: Methods and parameters used for the array processing.

5.2 Obtained dispersion curves

Both 1C and 3C (Fig. 8) analysis provided similar results. The Rayleigh fundamental mode could be picked between 1.4 and $10.8\,\mathrm{Hz}$ including its standard deviation. Velocities range from $730\,\mathrm{m/s}$ at $1.4\,\mathrm{Hz}$ down to $200\,\mathrm{m/s}$ at $10\,\mathrm{Hz}$. The radial component shows partly the Rayleigh mode, but was not used in the picking. The transverse component allows to pick the fundamental Love mode between 1.2 and $7.4\,\mathrm{Hz}$ including its standard deviation (Fig. 8). Velocities range from $550\,\mathrm{m/s}$ at $1.2\,\mathrm{Hz}$ down to $210\,\mathrm{m/s}$ at $7.4\,\mathrm{Hz}$. All dispersion curves are presented in Fig. 9.

Moreover, the SVD method allowed to derive the ellipticity of the Rayleigh mode [Poggi and Fäh, 2010], with resolution down to $0.8\,\mathrm{Hz}$ only. It compares well to the H/V ratios.

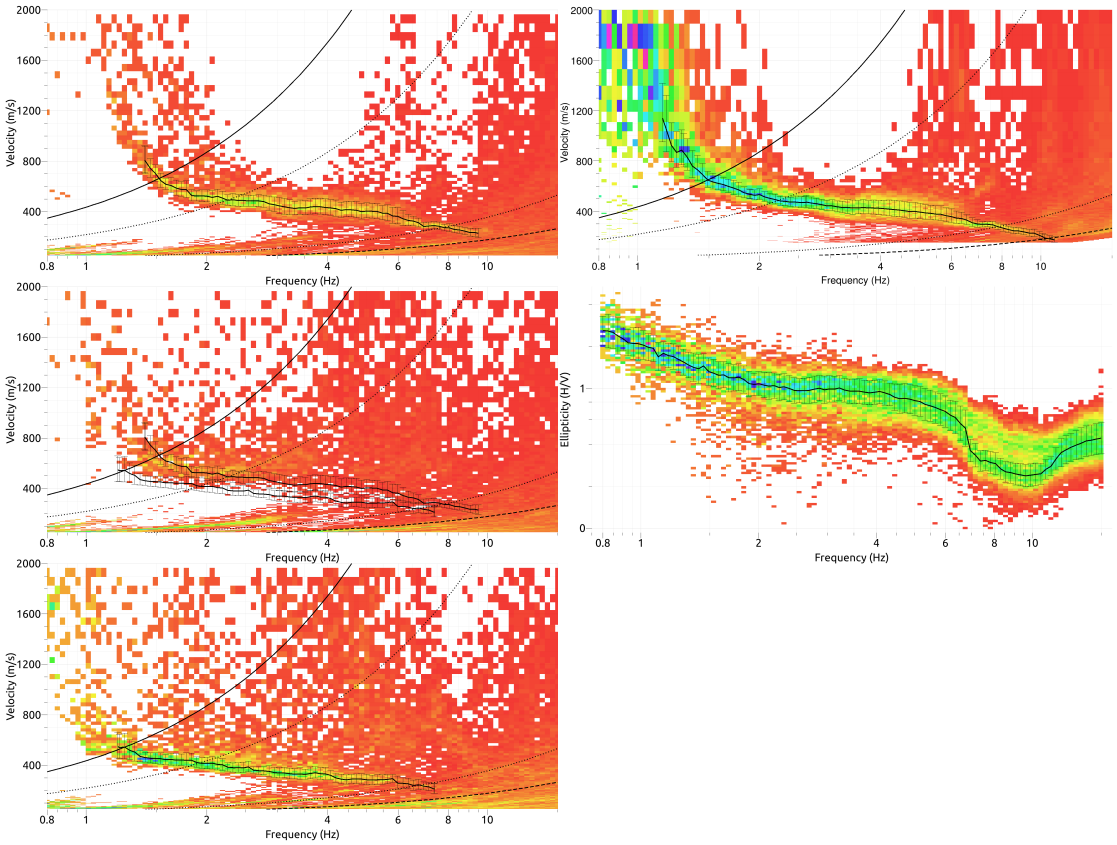

Figure 8: Dispersion curves and ellipticity obtained from the 1C (top right) and 3C array analysis (left and centre-right). Top: Vertical - Centre: Radial - Bottom: Transverse component

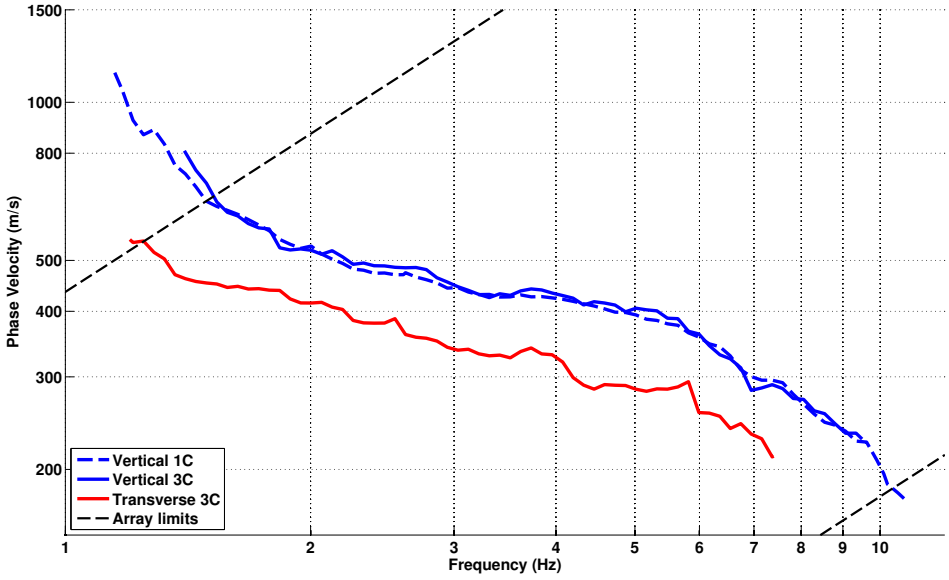

Figure 9: Picked dispersion curves from 1C and 3C analyses.

6 Inversion and interpretation

6.1 Inversion

For the inversion, the Rayleigh fundamental mode from the 1C analysis ($1.4 - 11\,\mathrm{Hz}$) and the Love fundamental mode ($1.3 - 7\,\mathrm{Hz}$) from the 3C FK analysis were used as simultaneous targets. The ellipticity peak ($0.6\,\mathrm{Hz}$) and curve are displayed in the results but not used in the inversion since 2D resonance probably occur at this site. All curves were resampled using 50 points between 0.3 and $20\,\mathrm{Hz}$ in log scale to force the code computing also the frequency band around the ellipticity peak.

The inversion was performed using the Improved Neighborhood Algorithm (NA) Wathelet [2008] implemented in the Dinver software. In this algorithm, the tuning parameters are the following: Ns_0 is the number of starting models, randomly distributed in the parameter space, Nr is the the number of best cells considered around these Ns_0 models, Ns is the number of new cells generated in the neighborhood of the Nr cells (Ns/Nr per cell) and It_{max} is the number of iteration of this process. The process ends with $Ns_0 + Nr * \frac{Ns}{Nr} * It_{max}$ models. The used parameters are detailed in Tab. 6.

It_{max}	Ns_0	Ns	Nr
500	10000	100	100

Table 6: Tuning parameters of Neighborhood Algorithm.

During the inversion process, low velocity zones were not allowed. The Poisson ratio was inverted in each layer in the range 0.2-0.4, except for the top part where is was allowed to go up to 0.47 (water table) and the density was supposed equal to $2000\,\mathrm{kg/m^3}$ except for the layer considered as rock ($2500\,\mathrm{kg/m^3}$). Inversions with free layer depths as well as fixed layer depths were performed. More layers than actually needed are used to smooth the obtained results and better explore the parameter space. 5 independent runs of 5 different parametrization schemes (5 and 6 layers over a half space and 11, 13 and 16 layers with fixed depth) were performed. For further elaborations, the best models of these 25 runs were selected (Fig. 12).

In the first $10\,\mathrm{m}$, a weak layer of about $200\,\mathrm{m/s}$ is found. The velocity at the surface may be even lower, but the measurement did not provide enough information on the high frequencies to constrain it. Below, the velocity increases (gradient shape) from 370 to $600\,\mathrm{m/s}$ down to the rock, at 150 to $200\,\mathrm{m}$ depth (with $180\,\mathrm{m}$ as a best estimate). Based on geology data (see the following section), this appears to be the interface with Molasse rock. The velocity in the bedrock is not constrained, the inversion pushing to the highest allowed value ($2000\,\mathrm{m/s}$), which is most probably too large.

When compared to the target curves (Fig. 10), the Love and Rayleigh modes are overall reproduced. The ellipticity peaks (first and second peaks) are reproduced by the H/V curve though the exact peaks are shifted, and the amplitude of the ellipticity is much higher in the models. The H/V curve may be related to 2D resonance that could explain this shift.

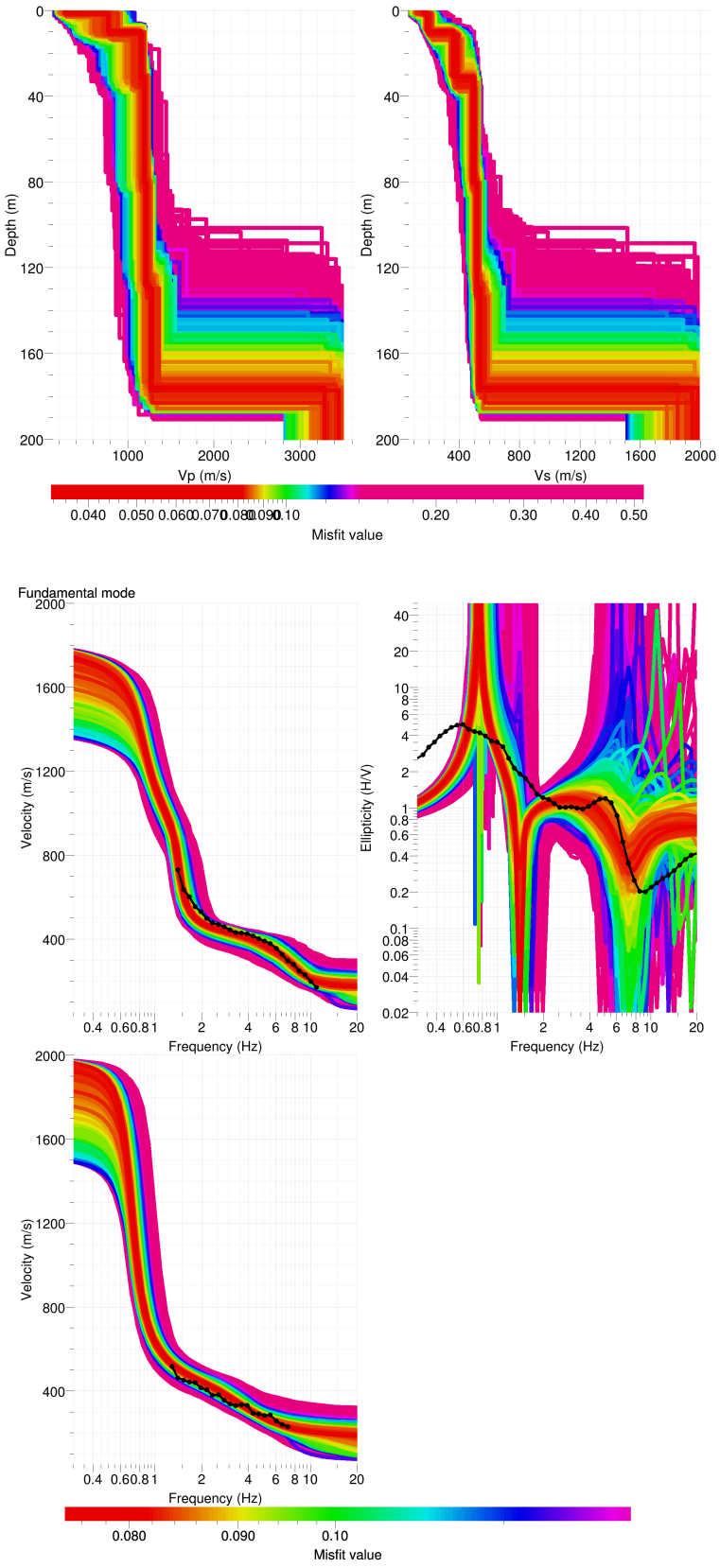

Figure 10: Inverted ground profiles in terms of V_p and V_s (top) and comparison between inverted models and measured Rayleigh and Love modes and corresponding ellipticity, free layer depth strategy.

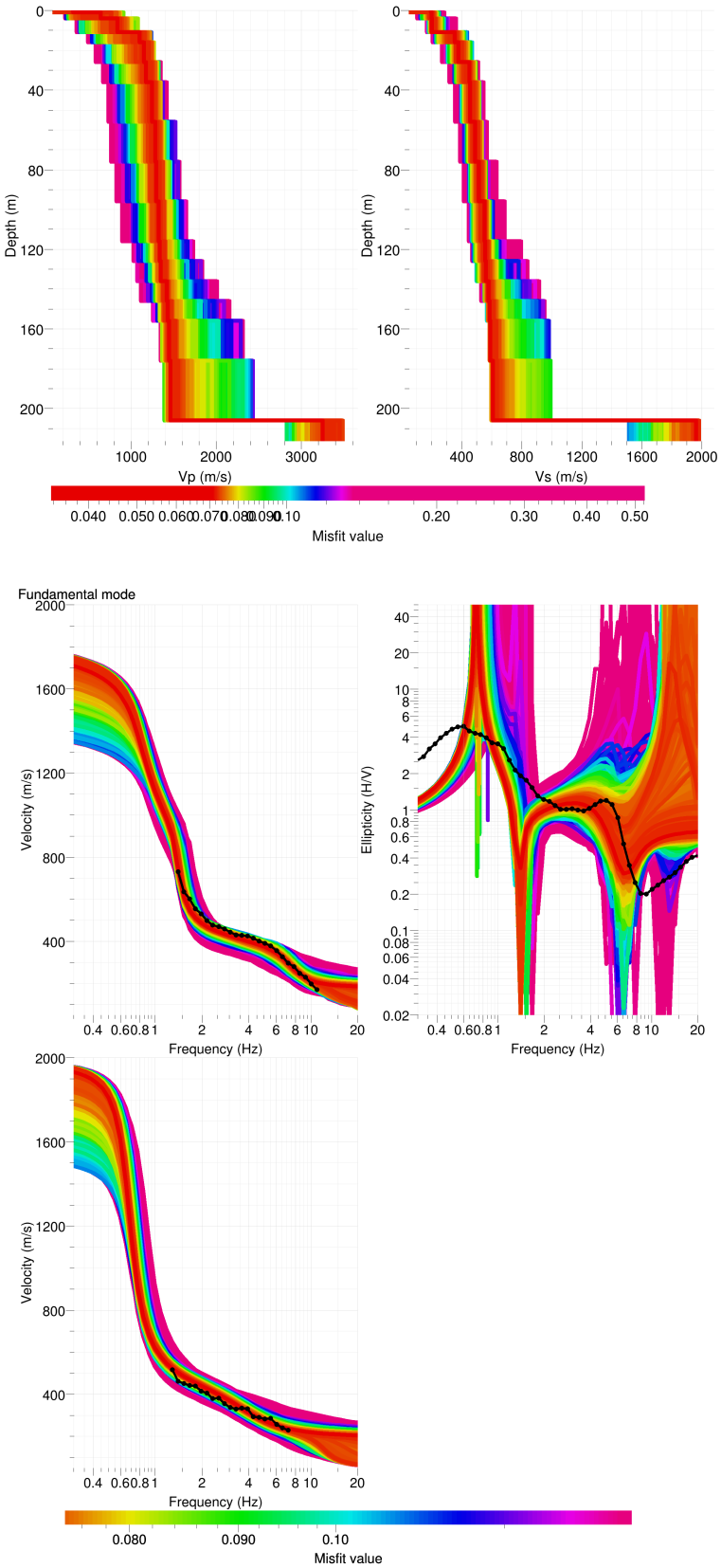

Figure 11: Inverted ground profiles in terms of V_p and V_s (top) and comparison between inverted models and measured Rayleigh and Love modes and corresponding ellipticity, fixed layer depth strategy.

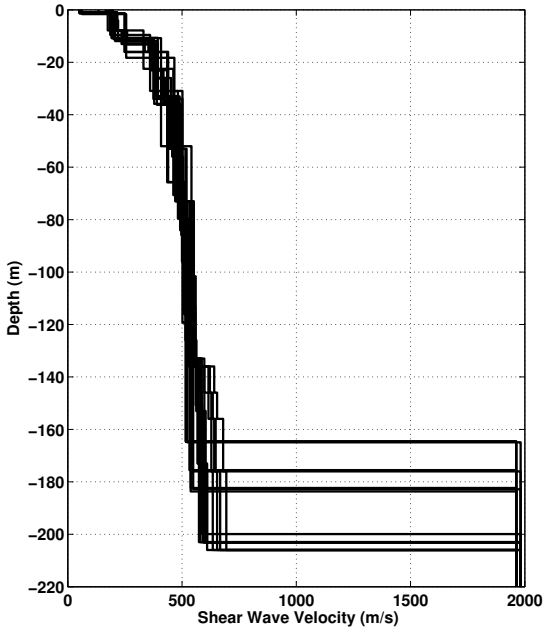

Figure 12: V_s ground profiles for the selected 25 best models.

6.2 Boreholes and interpretation

Three boreholes are available North of the station (Fig. 13). They all show glacial-lacustrine sediments on top of the Molasse bedrock. The Molasse is dipping to the South with a angle that can be estimated to be $9\,^\circ$ from these boreholes. Interpolating this angle leads to a depth of $150\,\mathrm{m}$ for station SOLB. The model of the quaternary sediments provided by Swisstopo (`http://www.geologieviewer.ch`) based on gravimetric anomaly inversion is coherent with these findings at this location with a depth of $140\,\mathrm{m}$ for the investigated site.

Borehole 1045 as well as the geology map show that the quaternary sediments are lacustrine for the SOLB site.

The soil column below the station SOLB is therefore interpreted as $10\,\mathrm{m}$ very low quality lacustrine sediments on top of around $170\,\mathrm{m}$ of glacial-lacustrine sediments (moraine). The Molasse is found at around $180\,\mathrm{m}$ depth.

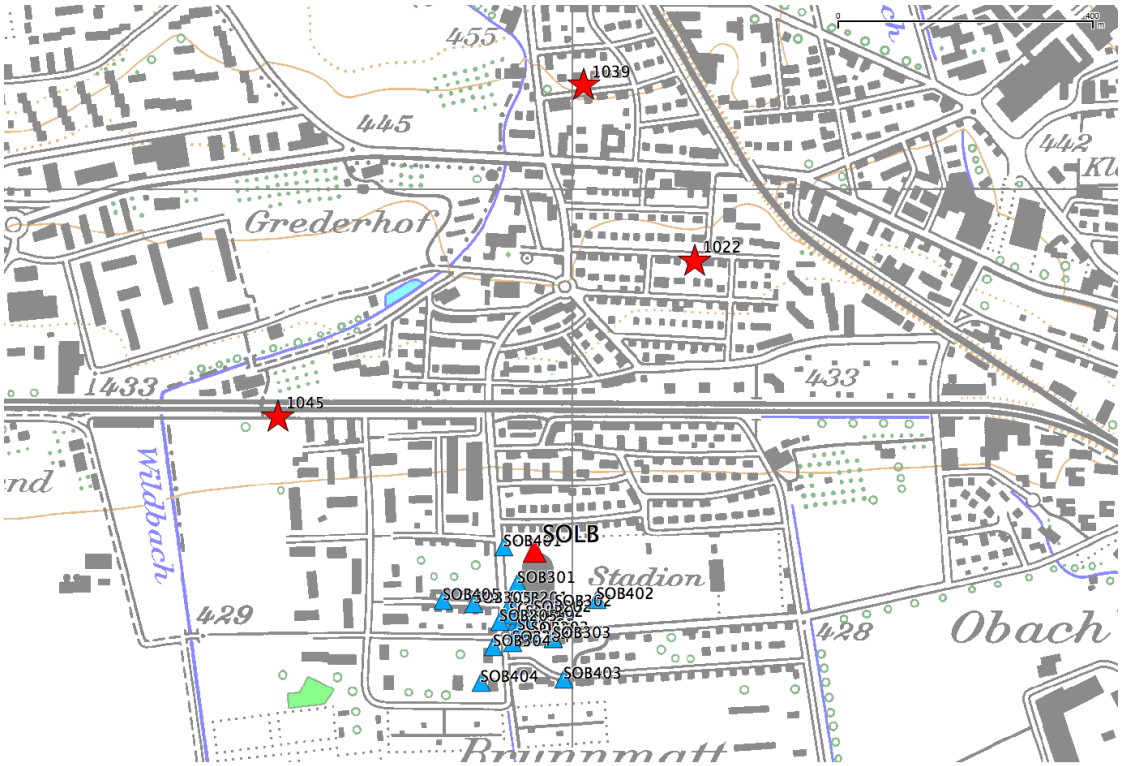

Figure 13: Map of boreholes close to the array.

6.3 Travel time average velocities and ground type

The distribution of the travel time average velocities at different depths was computed from the selected models. The uncertainty, computed as the standard deviation of the distribution of travel time average velocities for the considered models, is also provided, but its meaning is doubtful. $V_{s,30}$ is found to be $274\,\mathrm{m/s}$, which corresponds to class C in the Eurocode 8 [CEN, 2004] and D in the SIA261 [SIA, 2003]. The ground type map of the Federal Office for Environment (`www.map.bafu.admin.ch`) provides also type D at this site. Considering the first $10\,\mathrm{m}$ with a low velocity ($200\,\mathrm{m/s}$) and velocity below $10\,\mathrm{m}$ being greater than $400\,\mathrm{m/s}$, the site could be classified as class E in SIA261. It makes not really sense, though, since the basin is much deeper.

	Mean (m/s)	**Uncertainty (m/s)**
$V_{s,5}$	168	31
$V_{s,10}$	185	16
$V_{s,20}$	237	17
$V_{s,30}$	274	14
$V_{s,40}$	303	13
$V_{s,50}$	326	12
$V_{s,100}$	396	10
$V_{s,150}$	436	10
$V_{s,200}$	479	13

Table 7: Travel time averages at different depths from the inverted models. Uncertainty is given as one standard deviation from the selected profiles.

6.4 SH transfer function and quarter-wavelength velocity

The quarter-wavelength velocity approach [Joyner et al., 1981] provides, for a given frequency, the average velocity at a depth corresponding to 1/4 of the wavelength of interest. It is useful to identify the frequency limits of the experimental data (ellipticity peak at $0.6\,\mathrm{Hz}$ and minimum frequency in dispersion curves at $1.2\,\mathrm{Hz}$ here). The results using this proxy show that the dispersions curves constrain the profiles down to $75\,\mathrm{m}$ and no data is controlling the results below $190\,\mathrm{m}$ (Fig. 14). Moreover, the quarter wavelength impedance-contrast introduced by Poggi et al. [2012] is also displayed in the figure. It corresponds to the ratio between two quarter-wavelength average velocities, respectively from the top and the bottom part of the velocity profile, at a given frequency [Poggi et al., 2012]. It shows a trough (inverse shows a peak) at the resonance frequency.
Moreover, the theoretical SH-wave transfer function for vertical propagation [Roesset, 1970] is computed from the inverted profiles. It is compared to the quarter-wavelength amplification [Joyner et al., 1981], that however cannot take resonances into account (Fig. 15). In this case, the models are predicting a large amplification at clear resonance frequencies (0.7, 2, $3.1\,\mathrm{Hz}$...).

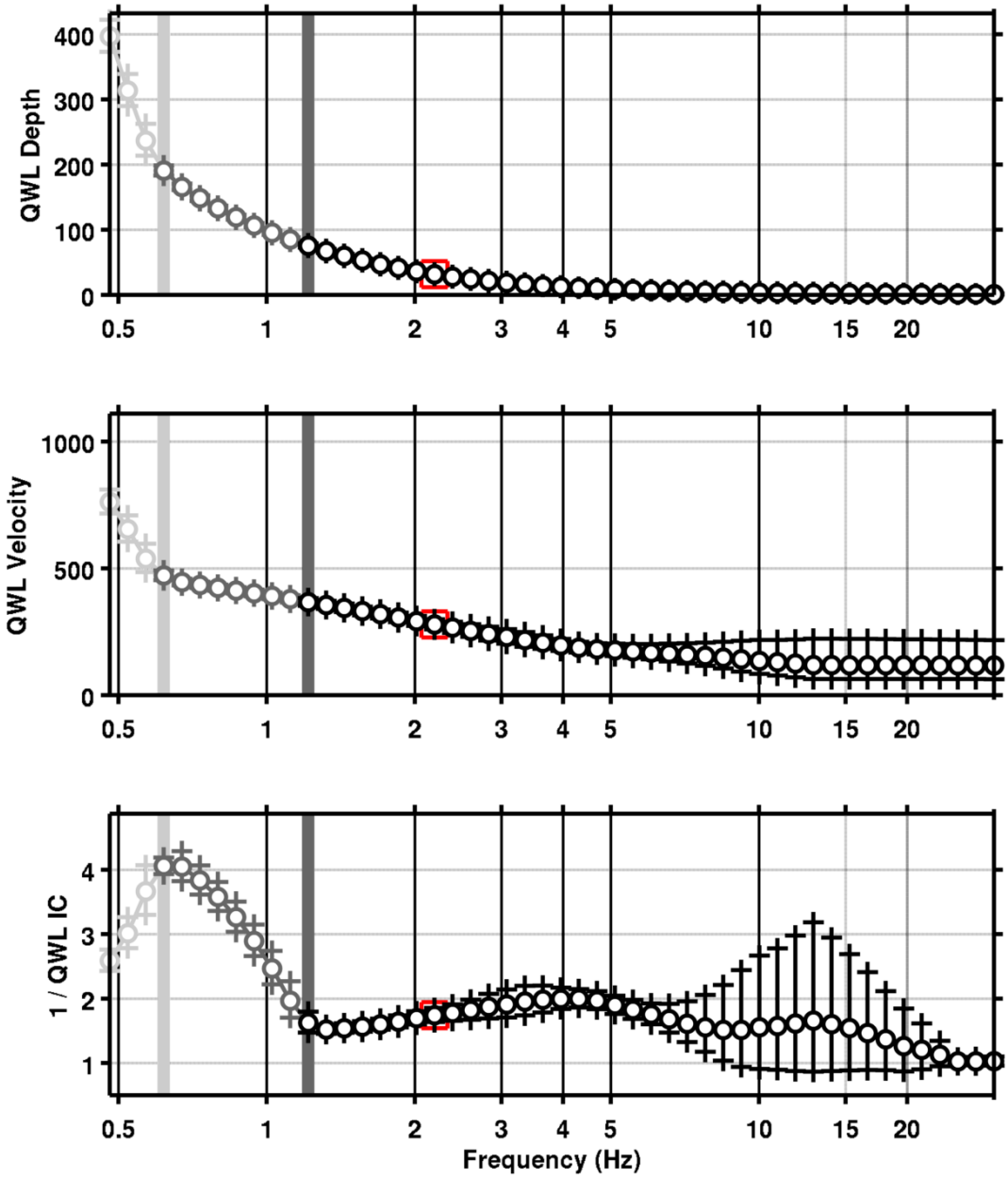

Figure 14: Quarter wavelength velocity representation of the velocity profile (top: depth, centre: velocity, bottom: inverse of the impedance contrast). Black curve is constrained by the dispersion curves, light grey is not constrained by the data. Red square is corresponding to $V_{s,30}$.

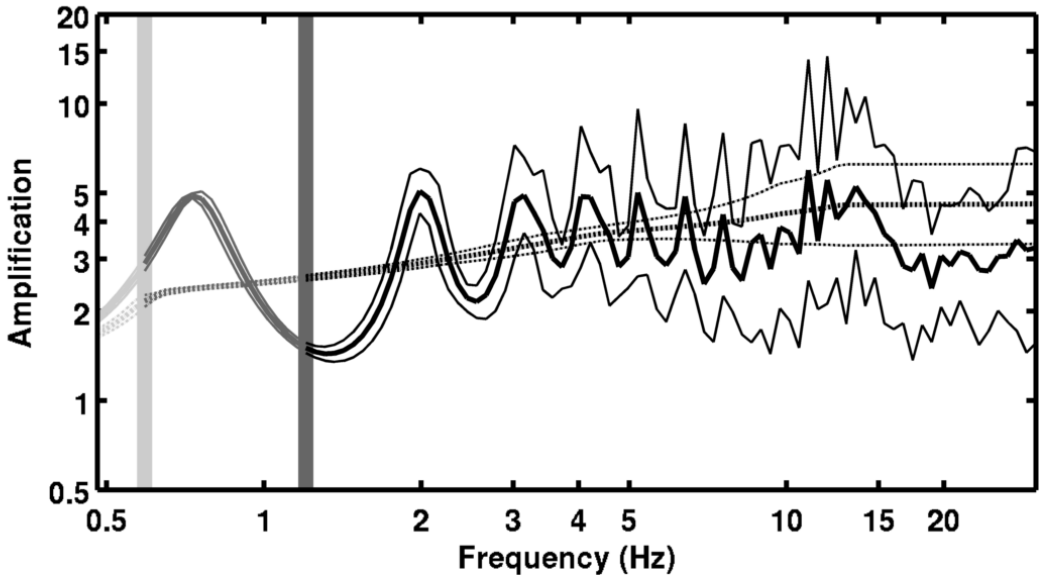

Figure 15: Theoretical SH transfer function (solid line) and quarter wavelength impedance contrast (dashed line) with their standard deviation. Significance of the greyshades is detailed in Fig. 14.

7 Conclusions

The array measurements presented in this study were successful in deriving a velocity model for the Brühl site in Solothurn, below the SOLB station. We found a first layer of weak lacustrine sediments of about $10\,\mathrm{m}$ with a shear wave velocity of about $200\,\mathrm{m/s}$. Below, moraine sediments with V_s from 370 to $600\,\mathrm{m/s}$ can be found down to an interface at $180\,\mathrm{m}$. This interface corresponds to the interface with the Molasse rock. The velocity in the Molasse is not constrained. Moreover, 2D resonance of the basin is suspected but the amplitude of the polarization is too low to definitely conclude. $V_{s,30}$ is found to be close to $274\,\mathrm{m/s}$. The EC8 and SIA261 ground types are C and D, respectively. Recordings on the new station will allow to validate the proposed 1D models and quantify the eventual 2D effects.

Acknowledgements

The authors thank Andrea Colombi for the help during these measurements and Céline Pittet from the Cantonal Office for Environment who provided borehole logs.

References

Sylvette Bonnefoy-Claudet, Fabrice Cotton, and Pierre-Yves Bard. The nature of noise wavefield and its applications for site effects studies. *Earth-Science Reviews*, 79(3-4): 205–227, December 2006. ISSN 00128252. doi: 10.1016/j.earscirev.2006.07.004. URL http://linkinghub.elsevier.com/retrieve/pii/S0012825206001012.

Jan Burjánek, Gabriela Gassner-Stamm, Valerio Poggi, Jeffrey R. Moore, and Donat Fäh. Ambient vibration analysis of an unstable mountain slope. *Geophysical Journal International*, 180(2):820–828, February 2010. ISSN 0956540X. doi: 10.1111/j.1365-246X.2009.04451.x. URL http://doi.wiley.com/10.1111/j.1365-246X.2009.04451.x.

J. Capon. High-Resolution Frequency-Wavenumber Spectrum Analysis. *Proceedings of the IEEE*, 57(8):1408–1418, 1969.

CEN. *Eurocode 8: Design of structures for earthquake resistance - Part 1: General rules, seismic actions and rules for buildings*. European Committee for Standardization, en 1998-1: edition, 2004.

Donat Fäh, Fortunat Kind, and Domenico Giardini. A theoretical investigation of average H / V ratios. *Geophysical Journal International*, 145:535–549, 2001.

Donat Fäh, Gabriela Stamm, and Hans-Balder Havenith. Analysis of three-component ambient vibration array measurements. *Geophysical Journal International*, 172(1):199–213, January 2008. ISSN 0956540X. doi: 10.1111/j.1365-246X.2007.03625.x. URL http://doi.wiley.com/10.1111/j.1365-246X.2007.03625.x.

Donat Fäh, Marc Wathelet, Miriam Kristekova, Hans-Balder Havenith, Brigitte Endrun, Gabriela Stamm, Valerio Poggi, Jan Burjanek, and Cécile Cornou. Using Ellipticity Information for Site Characterisation Using Ellipticity Information for Site Characterisation. Technical report, NERIES JRA4 Task B2, 2009.

William B. Joyner, Richard E. Warrick, and Thomas E. Fumal. The effect of Quaternary alluvium on strong ground motion in the Coyote Lake, California, earthquake of 1979. *Bulletin of the Seismological Society of America*, 71(4):1333–1349, 1981.

Katsuaki Konno and Tatsuo Ohmachi. Ground-Motion Characteristics Estimated from Spectral Ratio between Horizontal and Vertical Components of Microtremor. *Bulletin of the Seismological Society of America*, 88(1):228–241, 1998.

Valerio Poggi and Donat Fäh. Estimating Rayleigh wave particle motion from three-component array analysis of ambient vibrations. *Geophysical Journal International*, 180(1):251–267, January 2010. ISSN 0956540X. doi: 10.1111/j.1365-246X.2009.04402.x. URL http://doi.wiley.com/10.1111/j.1365-246X.2009.04402.x.

Valerio Poggi, Benjamin Edwards, and Donat Fäh. Characterizing the Vertical-to-Horizontal Ratio of Ground Motion at Soft Sediment-Sites. *Bulletin of the Seismological Society of America*, 102(6), 2012. doi: 10.1785/0120120039.

J.M. Roesset. Fundamentals of soil amplification. In R. J. Hansen, editor, *Seismic Design for Nuclear Power Plants*, pages 183–244. M.I.T. Press, Cambridge, Mass., 1970. ISBN 978-0-262-08041-5. URL http://mitpress.mit.edu/catalog/item/default.asp?ttype=2\&tid=5998.

SIA. *SIA 261 Actions sur les structures porteuses*. Société suisse des ingénieurs et des architectes, Zürich, sia 261:20 edition, 2003.

Marc Wathelet. An improved neighborhood algorithm: Parameter conditions and dynamic scaling. *Geophysical Research Letters*, 35(9):1–5, May 2008. ISSN 0094-8276. doi: 10.1029/2008GL033256. URL http://www.agu.org/pubs/crossref/2008/2008GL033256.shtml.